

### 3.7 Shocks in separated flows.

So far our discussion of shocks has concentrated on flows with finite layer thicknesses. However, the numerical simulations discussed in Section 3.4 reveal the existence of shocks in flows that are partially or completely separated from the left channel wall. The signature of these ‘transverse’ shocks is an abrupt change in the width of the stream that may propagate or remain stationary. We will begin the present discussion with the stationary version, an example of which is shown in Figure 3.7.1a.

An attempt to produce a hydraulic jump in a detached, laboratory flow was made by Pratt (1987). As suggested in Figure 3.7.2, fluid is pumped into the right-hand end of a channel, where it collects in a small reservoir and spills over an obstacle. Downstream of the sill, the flow becomes supercritical and terminates in a hydraulic jump. The subcritical flow downstream is withdrawn near the left-hand end of the channel. The procedure is to set up a steady state with no rotation, then spin up the channel to a steady rotation rate high enough to cause the supercritical flow to separate. An unavoidable difference between the laboratory flow and the numerical solution is that the ‘global’ deformation radius  $(gD_\infty)^{1/2} / f$  based on the reservoir depth  $D_\infty$  is much greater than the channel width  $w^*$  in the laboratory, but comparable to  $w^*$  in the numerical experiment. This is due to the fact that the laboratory experiments are performed with free-surface flows and full gravity. A Kelvin wave in the laboratory channel is therefore felt across the whole width. Separation is still possible because the deformation radius based on the local depth scale  $D$  of the supercritical flow can be much smaller than  $w$ .

The qualitative features of the classical planar hydraulic jump depend primarily on the Froude number  $V/(gD)^{1/2}$ , where the velocity and depth scales  $V$  and  $D$  are normally based on the approach flow. Rotation leads to the addition of at least one dimensionless parameter and a natural choice is the ratio of the upstream width scale  $W$  to the ‘local’ Rossby radius of deformation  $(gD)^{1/2} / f$  for the approach flow. If the approach flow is attached,  $W$  is just the dimensional channel width  $w^*$ . If the approach flow is detached then  $W$  is the separated current width  $w_e^*$  and  $V$  and  $D$  become related by geostrophic condition  $V = gD / fw_e^*$ . It follows that  $Wf / (gD)^{1/2} = (gD)^{1/2} / V$ , and thus the upstream flow is characterized by a single parameter. However, the downstream end state in this case may be attached, implying that  $w_e/w$  is a relevant parameter for the jump as a whole. A third possibility in which both end states are detached is generally not observed for a stationary jump. In summary, important parameters include the upstream value of  $V/(gD)^{1/2}$  along with<sup>1</sup> a second parameter

---

<sup>1</sup> Other parameters may be important as well. If the Rossby radius based on the potential depth  $D_\infty$  is comparable to  $w$  then the ratio of these lengths is relevant. If the potential vorticity of the approach flow varies, parameters measuring this variation may arise.

$$r = \begin{cases} w^* f / (gD)^{1/2} & \text{(completely attached)} \\ w^* / w_e^* & \text{(separated upstream, attached downstream)} \end{cases} \quad (3.7.1)$$

A representative sequence of experimental runs demonstrates the qualitative effects of increasing the rotation rate (Figure 3.7.3). The value of  $V/(gD)^{1/2}$  is held within the range  $7.1 \pm 0.5$  for all frames while  $r$  increases from 0.22 to 4.7. Frame (a) shows a case in which the rotation rate is small and the flow is indistinguishable from a non-rotating flow. The supercritical flow can be seen along with a hydraulic jump at the base of the obstacle. In Frame (b) the rotation rate has been increased to the point where some visual evidence of cross-channel variations in the flow field can be seen. In particular, the amplitude (depth change) of the jump is largest on the right side of the channel and waves along this edge have appeared downstream of the jump<sup>2</sup>. In Frames C and D, the supercritical flow has separated and the hydraulic jump is manifested primarily as a discontinuity in the width of the stream. The conjugate subcritical flow remains attached to the left wall, even at the highest rotation rates. A broad, cyclonic recirculation (not visible in the photos) forms downstream of the zone of reattachment. The abrupt reattachment and the downstream recirculation are similar to that observed in the numerical simulations (Figure 3.7.1a,b).

As  $r$  increases, the upstream-to-downstream increase in depth becomes less abrupt. For separated upstream flow, the transition in depth is smooth and wave-like, and the region immediately downstream of the transition is observed to contain turbulent, horizontal eddies. There is no visual evidence of the vertical turbulence and mixing that characterizes non-rotating jumps. These observations suggest that potential vorticity may be approximately conserved across the jump at higher values of  $r$ , but a shock-joining model based on this assumption fails to accurately predict the downstream state. The numerical simulations clearly show that potential vorticity is altered (Figure 3.7.1b and c), much of the implied dissipation occurring downstream of the point of reattachment.

Another feature that complicates the discussion of dissipation is that the detached laboratory flow is bordered by a shallow but relatively wide, viscous region. As shown by a cross section of the supercritical flow (crosses in Figure 3.7.4) the fluid immediately adjacent to the right wall is strongly banked and is well approximated by zero potential vorticity profile (solid line) for the same volume flux and inviscid width. To the left lies a broad, shallow area where the fluid depth is close to the characteristic Ekman layer thickness ( $2\nu/f$ ) based on the kinematic viscosity  $\nu$ .

Stationary shocks would appear to depend on the presence of a 'left' wall, even when the upstream flow is separated. Although this has not been proven in a general way, it is strongly suggested by the experiments described above. As shown by Nof (1984), this constraint is relaxed if the shocks are allowed to propagate. A possible

---

<sup>2</sup> This contrasts with attached numerical jumps (e.g. Figure 3.30), which have maximum amplitude on the left side of the channel. However the differences may be due to the differences in the Kelvin wave decay scale  $(gD_\infty)^{1/2} / f$ , which is  $\ll w$  in the numerical simulation and  $\gg w$  in the laboratory experiment.

version of such a feature consists of an expansion, both in width and depth, of a coastal current (Figure 3.7.5). The fluid is assumed to have zero potential vorticity and also have positive velocity, so that the current is supercritical (in view of the Section 3.2.3 discussion). A shock is postulated as a result of an increase in the transport, and therefore the wall depth, at some point far upstream. The resulting disturbance is imagined to steepen in the manner described in section 2.3, eventually breaking and forming a steadily propagating discontinuity in depth that moves towards the observer.

Nof joins the end states of the shock using conservation of potential vorticity and width-integrated mass and momentum, even though the first constraint is not strictly justified. The calculation is further constrained by the requirement that the energy of fluid parcels cannot increase as they pass through the jump. This last condition rules out any solution for which fluid passes across the shock from deeper to shallower depths, meaning that the fluid velocity  $v$  in the moving frame of the shock must be  $<0$  for all  $x$ . The resulting theory gives a prediction of one end state given the other end state and the propagation speed. Or, the shock speed can be predicted from the knowledge of one end state and the change in wall depth. It is found that the shock speed is always greater than  $(gd_d^*)^{1/2}$  based on the wall depth  $d_d^*$  of the flow into which the shock propagates. Stationary shocks are therefore disallowed. As in non-rotating analogs of this shock, the propagation speed is greater than that of the linear wave propagating in the downstream region, but slower than the linear wave propagating down stream in the upstream region. This *must* be true to remain consistent with the steepening process that forms the shock in the first place.

The width is always increased by the passage of the shock (e.g. Figure 3.7.6) and this makes the solutions quite different from the transverse shocks found in the numerical simulations of Section 3.4. As exemplified by the feature shown at  $y=18$  at  $t=20$  in Figure 3.4.6, the numerically generated shock involve a *decrease* in width. Nof's solutions involve large depth changes along the wall that propagate at a speed comparable to  $(gd^*(w^*/2))^{1/2}$ ; both these features suggest Kelvin wave dynamics. The shocks in Figure 3.4.6 involve considerable changes in width accompanied by minor changes in depth, suggesting frontal wave dynamics. 'Frontal bores' are apparently not admitted in Nof's theory, perhaps due to the restriction to unidirectional velocity in both end states.

At the time of this writing, no direct observations of transverse shocks or jumps had been made in the ocean or atmosphere. Such features would occur internally and would possibly involve exchange of mass and momentum between layers, a process not accounted for in the above formulations. In the Denmark Strait, for example, the supposedly supercritical outflow gradually descends into the deep North Atlantic, gradually entraining overlying water as it does so. There is no evidence of a rapid, stationary change in the width of the flow. The suggestion that contact with the left channel wall is necessary for a stationary jump would mean that the jump would have to occur within the strait and not in the downstream basin. Observations in the Vema Channel (Hogg, 1983) reveal the type of rapid energy transformation that could be caused by a hydraulic jump, though there is no clear connection with the structural features of

the jumps discussed above. In a classical jump one expects the fluid depth, and therefore the potential energy, of the flow to increase in as the fluid passes through the jump. (Total energy is, of course, lost.) Hogg calculated the potential energy using hydrographic measurements taken along three different streamlines of the observed flow (solid curves in Figure 3.7.7). The streamlines are defined by intersections between potential density ( $\sigma_4$ ) surfaces and the bottom. For the streamlines corresponding to potential density  $\sigma_4=46.11$  and  $46.13$ , the potential energy decreases and then increases as it would if an accelerating supercritical flow passed through a jump.

### Exercises:

1. Consider a hypothetical stationary shock wave in which the upstream state is supercritical, the downstream state is subcritical, and both are detached and have zero potential vorticity. Show (as Nof, 1984 did) that such a feature cannot be stationary.
2. Give a plausible reason that explains why Nof's (1984) shock solutions apparently do not include breaking frontal waves.

### Figure Captions:

3.7.1 (a) Contours of surface elevation in the vicinity of a transverse hydraulic jump. The flow is left-to-right and is spilling down an obstacle whose crest lies at  $y=0$  and  $w=2$ . The shaded region indicates dry channel bottom. (b) Potential vorticity distribution for the flow in (a). (c) Potential vorticity  $q(\psi)$  distributions across sections A and B as marked in (a). From Pratt et al. (2000).

3.7.2 Laboratory apparatus for rotating hydraulic jump experiment. (From Pratt, 1987.)

3.7.3 Photos of hydraulic jumps for (a)  $r=0.22$ , (b)  $r=0.84$ , (c)  $r=3.10$ , (d)  $r=4.7$ . The supercritical flow is spilling from right to left down an obstacle lying to the right in each photo. In (c) and (d) the supercritical flow has separated from the near wall. The Froude number  $V/(gD)^{1/2}$  of the supercritical flow just upstream of the jump is  $7.1\pm 0.5$  in all cases. The value of  $V$  is estimated from the geostrophic relation as  $g\Delta d^*/fw^*$ , where  $\Delta d^*$  is the change in depth across the stream and  $w$  is the width (either separated or attached) of the flow.  $D$  is the average of the depths on the two sides of the stream. (From Pratt, 1987)

3.7.4 Cross section of the supercritical flow shown in Figure 3.7.3c. The crosses indicate measurements of the free surface elevation. The solid line shows the free surface profile of a zero potential vorticity flow with the same volume flow rate and same width. The width in this case is taken as the distance from the right wall at which the depth falls beneath the Ekman thickness ( $2\nu/f$ ), as shown by the dashed line. All depths are nondimensionalized by the observed wall depth and the cross-channel coordinate  $x$  by the observed inviscid width  $w_e^*$ . (Pratt, 1987, Fig. 5)

3.7.5 Sketch of hypothetical shock wave in a separated current. The observer faces upstream (-y). (based on Nof, 1984, Figure 3a)

3.7.6 Example of the upstream and downstream depth profiles for a forward propagating shock in a separated current with zero potential vorticity. The Froude number  $\bar{F}=1$  and the downstream wall depth is 0.3 times the upstream wall depth. The Froude number is defined by  $\bar{F} = (v_1^* (w^*/2) + v_1^* (w_e^*)) / (2gd_d^*)^{1/2}$ , where  $v_1(w^*/2)$  and  $v_1(w_e^*)$  are the values of  $v^*$  on the two edges of the downstream current (ahead of the shock) and  $d_d^*$  is the downstream wall depth. (Based on Figure 10 of Nof, 1984)

3.7.7 Effective potential energy along three streamlines of the deep Vema Channel overflow. The streamlines are defined as intersections between the indicated potential density ( $\sigma_4$ ) surfaces and the bottom. The lower the value of  $\sigma_4$ , the closer the streamline is to the west wall. The flow is to the right in the figure and horizontal distance is measured downstream from the mouth, where the channel joins with the Argentine Basin. Speed arrows are those needed to make the total energy of the 46.10 surface uniform. (From Hogg, 1983)

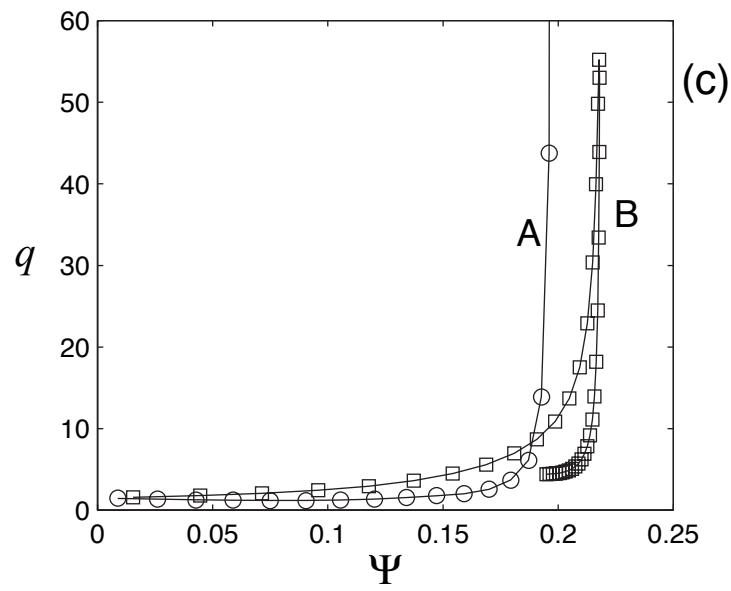
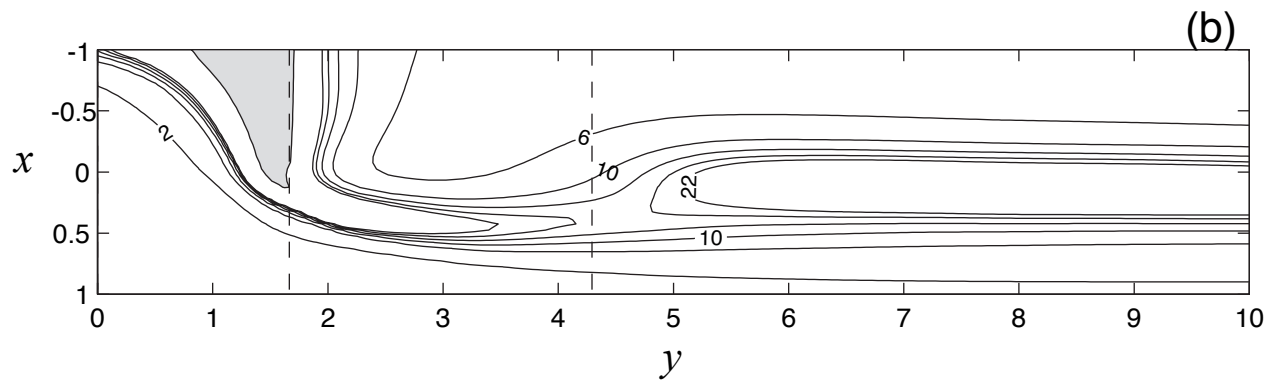
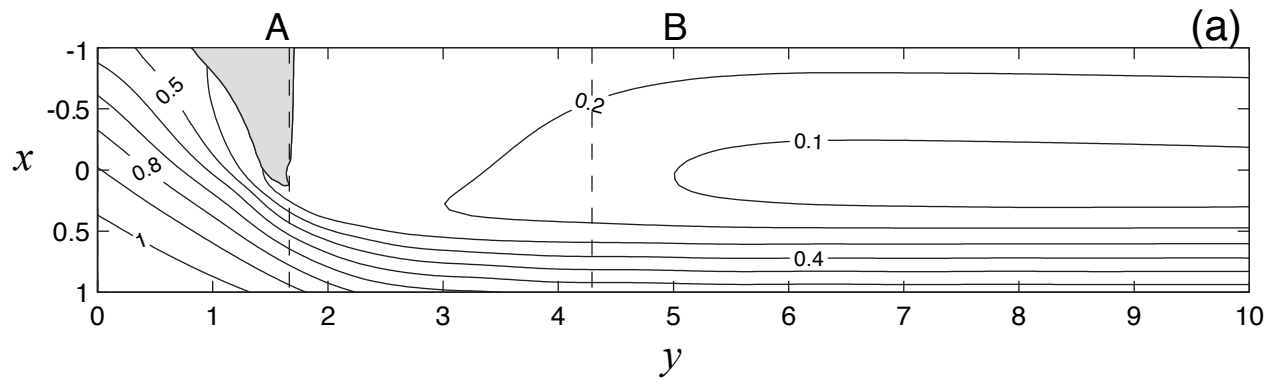


Figure 3.7.1

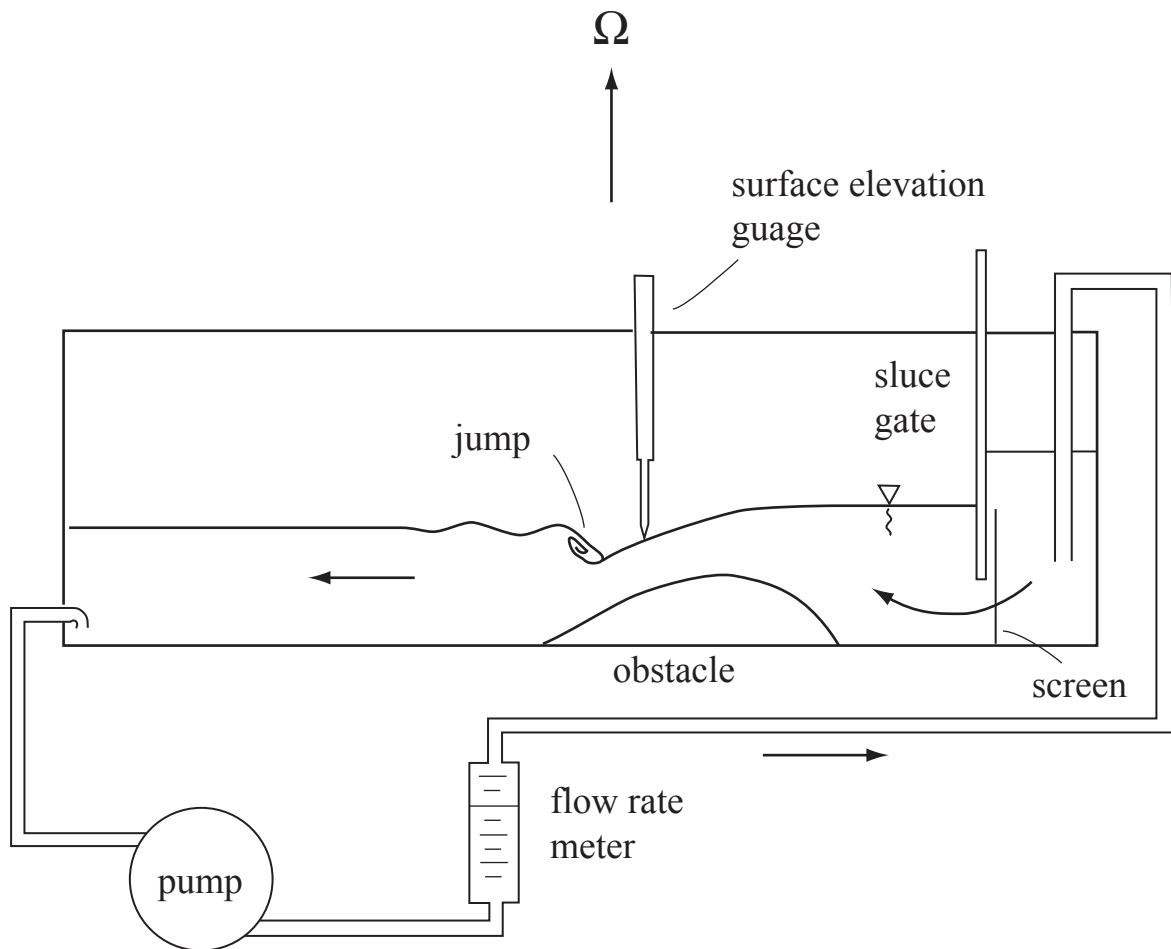


Figure 3.7.2

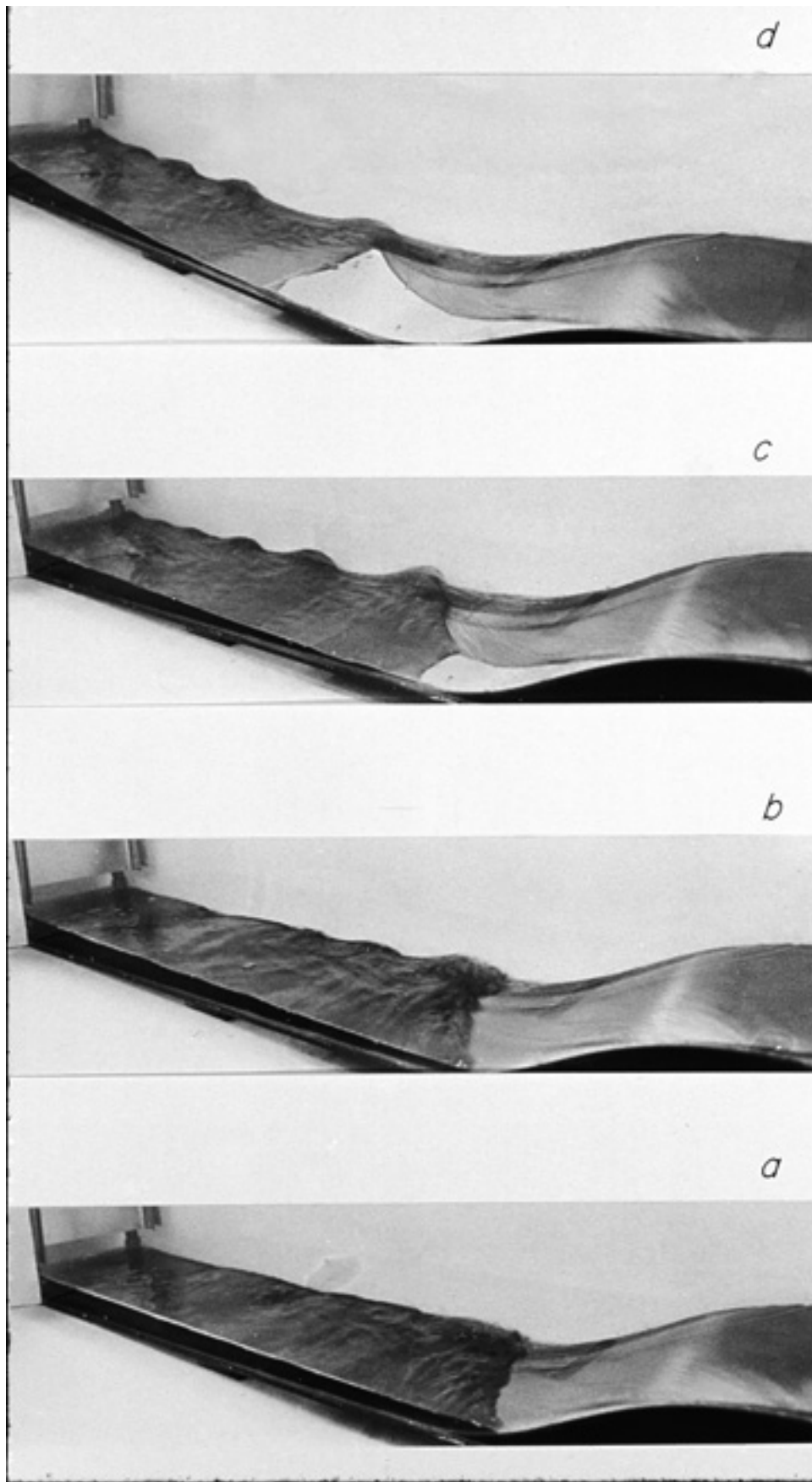


Figure 3.7.3

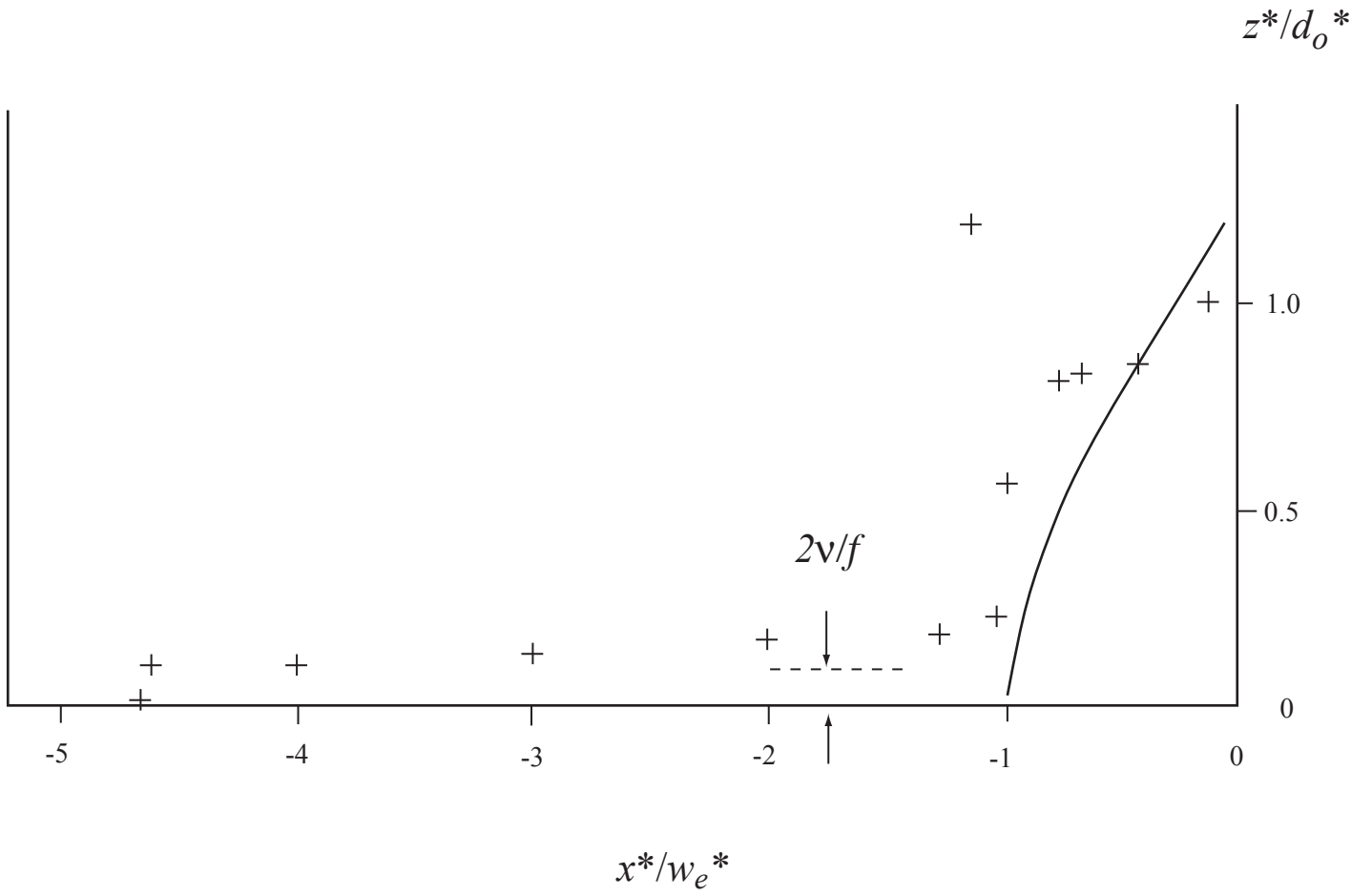
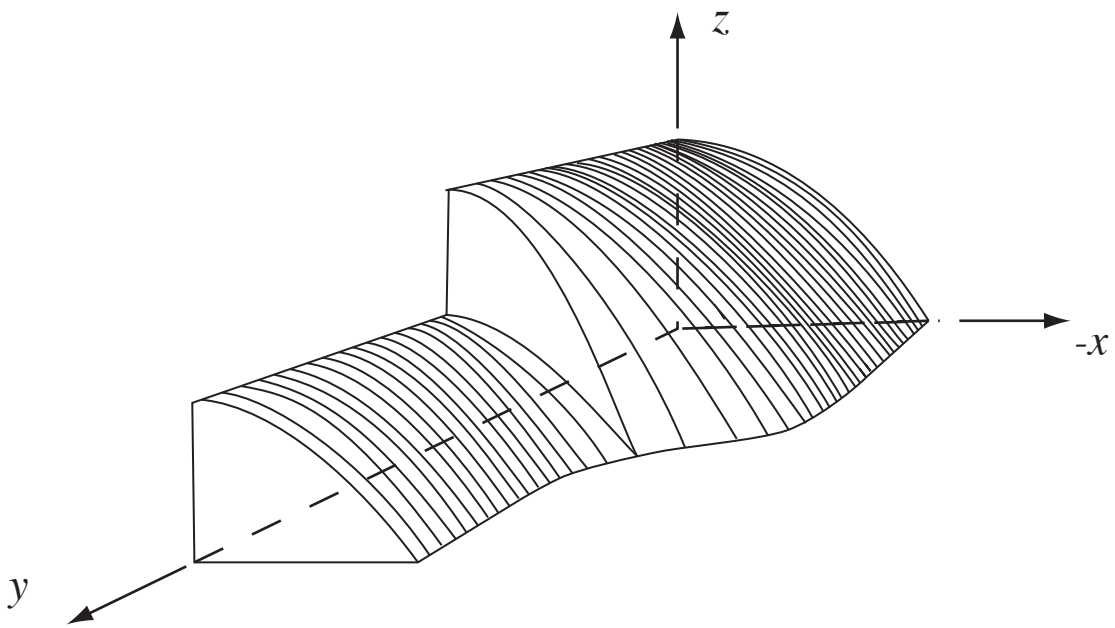


Figure 3.7.4



*Figure 3.7.5*

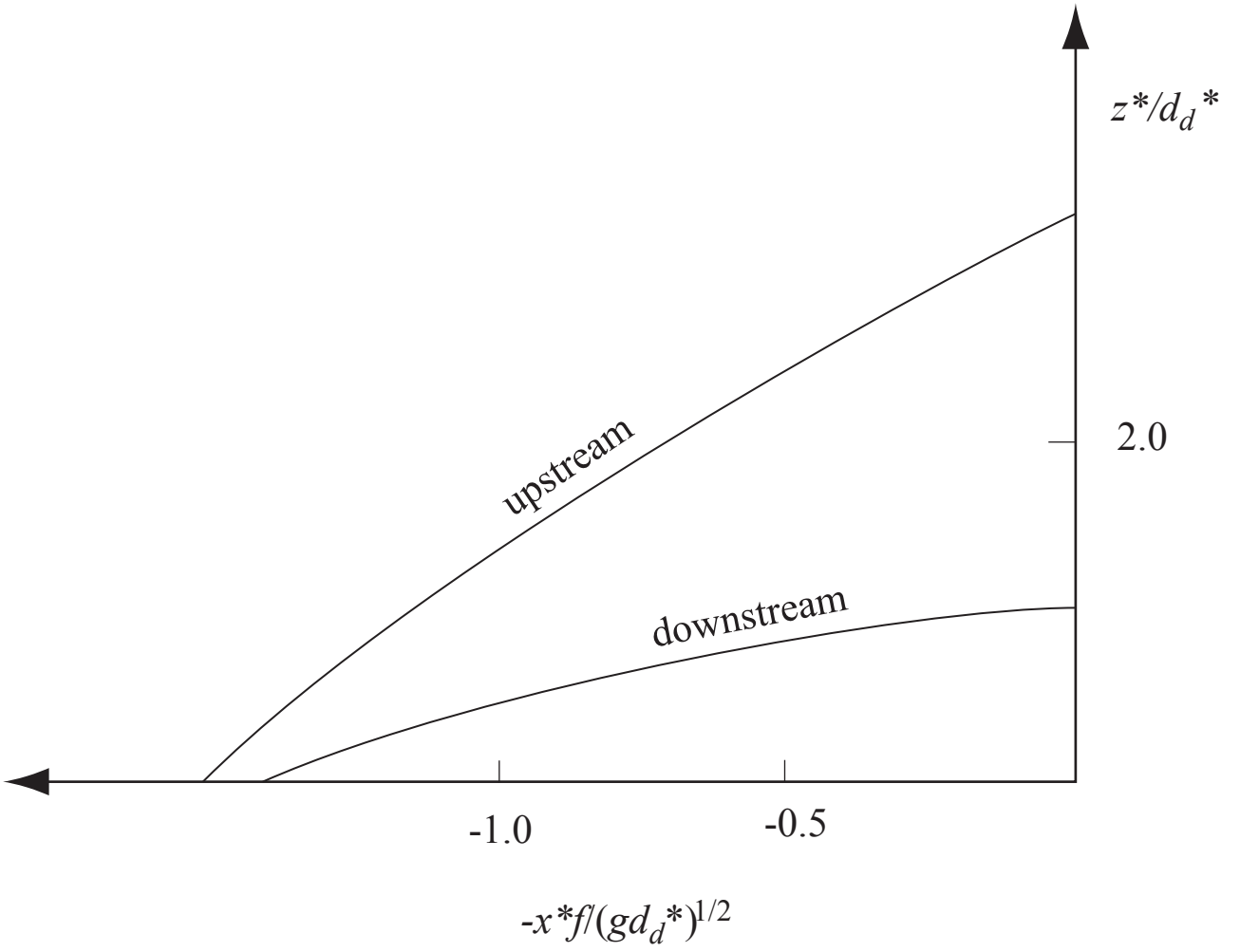


Figure 3.7.6

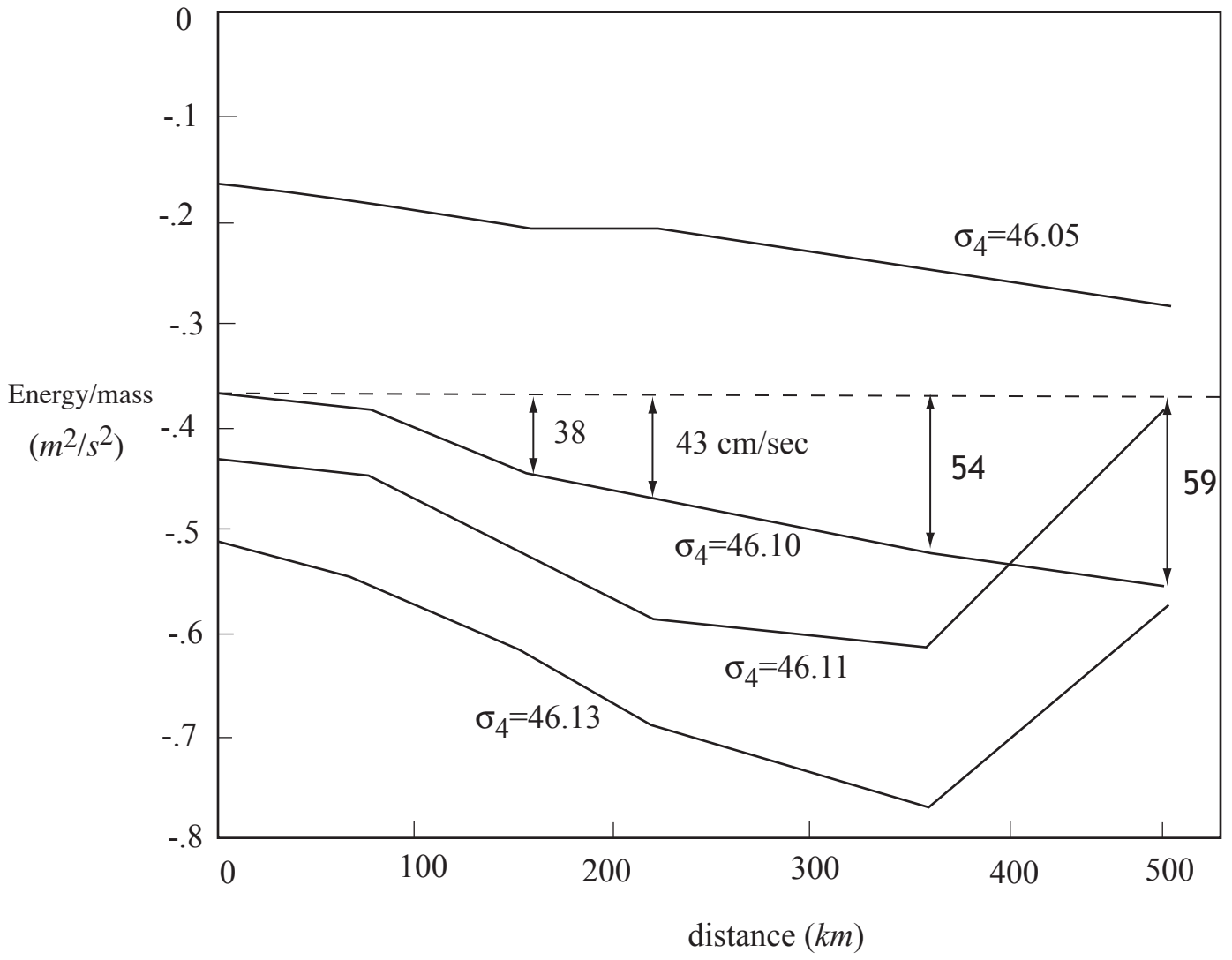


Figure 3.7.7